NASA Technical Memorandum 86812

Prediction of Service Life of Aircraft Structural Components Using the Half-Cycle Method

William L. Ko

May 1987

NASA

National Aeronautics and
Space Administration

Prediction of Service Life of Aircraft Structural Components Using the Half-Cycle Method

William L. Ko
Ames Research Center, Dryden Flight Research Facility, Edwards, California

1987

SUMMARY

The service life of aircraft structural components undergoing random stress cycling was analyzed by the application of fracture mechanics. The initial crack sizes at the critical stress points for the fatique-crack growth analysis were established through proof load tests. The fatique-crack growth rates for random stress cycles were calculated using the half-cycle method. A new equation was developed for calculating the number of remaining flights for the structural components. The number of remaining flights predicted by the new equation is much lower than that predicted by the conventional equation.

INTRODUCTION

Aircraft structural components commonly contain flaws, defects, or anomalies of various shapes; these either are inherent in the basic material or are introduced during the manufacturing and assembly processes. A large percentage of service cracks found in aircraft structures are initiated from crack nucleation sites such as tool marks, manufacturing defects, and surface microinclusions (ref. 1). Under the combined influences of environment and service loading, these flaws may grow to reach catastrophic sizes, resulting in serious reduction of service life or complete loss of the aircraft. Thus, to a great extent, the integrity of the aircraft structure is dependent upon the safe and controlled growth of cracks as well as the achievement of residual strength in their presence.

The operational life (service life) of aircraft structural components is affected by the magnitude and cumulative effects of external loads coupled with any detrimental environmental action. The presence of moisture, chemicals, suspended contaminants, and naturally occurring elements such as rain, dust, and seacoast atmosphere can cause deterioration in structural strength due to premature cracking and acceleration of subcritical crack growth (refs. 2 and 3).

As aircraft structures begin to age (that is, as flight hours accumulate), existing subcritical cracks or new cracks can grow in some high-stress points of the structural components. The usual approach is to inspect the structures periodically at certain intervals. However, even after inspection there may be some undetected cracks in a structure. To ensure that the structure still has integrity for future flights, proof load tests are usually conducted on the ground. The purpose of proof load tests is to load a structure to certain proof load conditions (slightly lower than the design limit load conditions) to test its integrity. If there should exist undetected cracks in the structural component that are larger than the critical crack sizes, that structural component will surely fail during the proof load tests and will be replaced. This process can reduce the chance of catastrophic accidents during flight. If all structural components survive the proof load tests, then fracture mechanics can be applied to estimate fatigue life (number of remaining flights) for each critical structural component by using the initial crack size established for each structural component during the proof load tests and then using the stress cycles (obtained through strain gage measurements) for each structural component during the first flight after the proof load tests.

This report describes the application of fracture mechanics and the half-cycle method to calculate the number of remaining flights for aircraft structural components.

The author gratefully acknowledges contributions by William W. Totton and Jules M. Ficke of Synernet Corp. in setting up computer programs for flight data reductions and crack growth computations.

SYMBOLS

A	crack location parameter
a	crack length of edge crack, one-half the crack length of through-thickness crack, or depth of surface crack
a_ℓ	crack size (length or depth) after the ℓth flight
a_c^o	limit crack length (or depth) associated with the operational peak load
a_c^p	initial fictitious crack length (or depth) established by the proof load tests
C	material constant in Walker crack growth rate equation
c	half-length of surface crack
E	complete elliptic function of the second kind
F_ℓ	number of remaining flights after the ℓth flight
$\bar{F}_\ell$	number of remaining flights after the ℓth flight predicted from the newly developed equation of remaining flights
f	operational peak stress factor (f < 1)
i	integer associated with half-cycles, or critical stress points
j	integer associated with half-cycles
K_I	Mode I stress intensity factor
K_{I_c}	Mode I critical stress intensity factor
K_{max}	Mode I stress intensity factor associated with σ_{max}, $AM_K \sigma_{max} \sqrt{\pi a/Q}$

2

k	modulus of elliptic function
ℓ	integer associated with flights
M_K	flaw magnification factor
m	Walker exponent associated with K_{max}
N	number of stress cycles available for operations
N_ℓ	number of stress cycles used during the ℓth flight
n	Walker exponent associated with stress ratio R
Q	surface flaw shape and plasticity factor
R	stress ratio, $\sigma_{min}/\sigma_{max}$
t	thickness of plate
V_A	front hook vertical load
V_{BL}	left rear hook vertical load
V_{BR}	right rear hook vertical load
Δa_ℓ	amount of crack growth during the ℓth flight
δa_i	crack growth increment resulting from one cycle of constant-amplitude stress cycling under loading magnitude of ΔK_i and R_i
ΔK	Mode I stress intensity amplitude, $AM_K(\sigma_{max} - \sigma_{min})\sqrt{\pi a/Q}$
σ_∞	remote uniaxial tensile stress
σ_∞^o	uniaxial tensile stress associated with the peak operational load level
σ_∞^P	proof tensile stress induced by the proof loads
σ_i	tensile stress at critical stress point i
σ_i^*	peak value of σ_i induced by the proof loads
σ_{max}	maximum stress of the stress cycle
σ_{min}	minimum stress of the stress cycle

σ_U tensile strength

σ_Y yield stress

τ_U ultimate shear strength

ϕ angular coordinate for semielliptical surface crack

THEORY

Fracture Mechanics

The top part of figure 1 shows the most common types of cracks: through-thickness crack, surface crack, and edge crack. According to fracture mechanics, the stress intensity factor K_I for the Mode I deformation (tension mode) associated with any type of crack can be expressed as

$$K_I = AM_K\sigma_\infty\sqrt{\frac{\pi a}{Q}} \tag{1}$$

where A is the crack location parameter (A = 1 for the through-thickness crack, A = 1.12 for both the surface and the edge cracks (see fig. 1)); M_K is the flaw magnification factor (for a very shallow crack $M_K = 1$; as the depth of the crack reaches the back surface of the plate, $\dot{M}_K = 1.6$ (see fig. 1)); σ_∞ is the remote uniaxial tensile stress; a is one-half the crack length for the through-thickness crack, or the length of the edge crack, or the depth of the surface crack (see fig. 1); and Q is the surface flaw shape and plasticity factor given by

$$Q = [E(k)]^2 - 0.212 \left(\frac{\sigma_\infty}{\sigma_Y}\right)^2 \tag{2}$$

where σ_Y is the yield stress and E(k) the complete elliptic function of the second kind, defined as

$$E(k) = \int_0^{\pi/2} \sqrt{1 - k^2 \sin^2 \phi} \, d\phi \tag{3}$$

where ϕ is the angular coordinate for a semielliptical surface crack, defined in figure 1, and the modulus k of the elliptic function is defined by

$$k = \sqrt{1 - \left(\frac{a}{c}\right)^2} \tag{4}$$

where c is the half-length of the surface crack (see top center of fig. 1).
The bottom part of figure 1 shows the plots of a/2c as functions of Q for dif-

4

ferent values of σ_∞/σ_Y and the plot of M_k as a function of a/t, where t is the plate thickness.

Proof Load Tests

The purpose of proof load tests is to load the entire aircraft structure (or its components) to certain proof load levels to test structural integrity and to establish initial fictitious crack sizes associated with critical structural components for fatigue life analysis. The proof load levels are usually slightly lower than the design limit load conditions associated with different maneuvers. If there exists in a certain structural component a previously undetected crack that is larger than the critical crack size associated with the proof load, that component will certainly fail during the proof load tests and will be replaced. Thus, a catastrophic accident during flight can be avoided. If the entire structure survives the proof load tests, then the critical stress point of the structural component has been subjected to a proof tensile stress σ_∞^P induced by the proof loads. If K_{I_C} denotes the critical stress intensity factor (or material fracture toughness) of the structural component material, the maximum crack length a_c^P the structural component can carry under the proof loads without failure (or rapid crack extension) may be calculated from equation (1) by setting $K_I = K_{I_C}$, and $\sigma_\infty = \sigma_\infty^P$. In reality, there may not be any cracks that developed during proof tests; however, it is assumed that a fictitious crack of length a_c^P has been created at the critical stress point of the structural component during the proof load tests. During actual operations, the structural component will be subjected to much lower stress levels than the proof stress level σ_∞^P. If σ_∞^O is defined as the peak operational stress level (highest peak of the stress cycles), then according to equation (1), the structural component can carry a fictitious crack of size a_c^O, which is much larger than a_c^P. The value a_c^O thus determined is considered to be the limit crack size toward which the initial crack a_c^P is allowed to grow after repeated operations. The crack size difference, $a_c^O - a_c^P$, is then the crack size increase permitted for the structural component in repeated operations. The left-hand plot in figure 2 shows crack length, a, as a function of normalized stress σ_∞/σ_U, where σ_U is the tensile strength of the material. It is seen that the lower the operational stress level, the larger the limit crack size available for the structural component. The right-hand plot in figure 2 shows crack length, a, as a function of number of constant stress cycles N.

Remaining Flights

If the structural component is cycled under constant stress amplitude (an idealized case for the purpose of discussion) for N_1 cycles during the first flight with the associated crack growth of Δa_1, then the number of remaining flights F_1 before

the limit crack size is reached may be estimated from the following conventional equation (see fig. 2):

$$F_1 = \frac{a_c^o - a_c^P}{\Delta a_1} = \frac{N}{N_1} \tag{5}$$

Equation (5) is based on the assumption that the amount of crack growth per flight for all subsequent flights will be equal to Δa_1 of the first flight. In reality, the amount of crack growth per flight will steadily increase with the number of flights accumulated, and the actual number of remaining flights will be less than the value F_1 predicted by equation (5) if the number of remaining flights is large (that is, $F_1 \gg 1$). As discussed in the following section, for a relatively low range of F_1, equation (5) may give a reasonably accurate prediction of the number of remaining flights. The amount of crack growth Δa_1 in equation (5) may be calculated from the following Walker equation (refs. 4 to 6) for fatigue-crack growth rate under constant-amplitude stress cyclings:

$$\frac{da}{dN} = C(K_{max})^m (1 - R)^n = C(\Delta K)^m (1 - R)^{n-m} \tag{6}$$

where C, m, and n are material constants, and K_{max}, ΔK, and R are respectively maximum stress intensity factor, stress intensity amplitude, and stress ratio, given by

$$K_{max} = AM_K \sigma_{max} \sqrt{\frac{\pi a}{Q}} \tag{7}$$

$$\Delta K = AM_K (\sigma_{max} - \sigma_{min}) \sqrt{\frac{\pi a}{Q}} \tag{8}$$

$$R = \sigma_{min}/\sigma_{max} \tag{9}$$

where σ_{max} and σ_{min} are respectively the maximum and the minimum stresses of the constant-amplitude stress cycles.

In reality, the stress cycles encountered during operations at the critical stress points of the structural component are not constant-amplitude stress cycles. To apply equations (6) to (9) to variable-amplitude stress cycles, different methods must be developed. In this report a half-cycle method (refs. 7 to 10) is used in the calculation of the fatigue-crack growth rate for variable-amplitude stress cycles.

Half-Cycle Theory

The top part of figure 3 shows an example of random stress cycles (variable-amplitude loading history). The stress history curve is the combination of a series of both increasing and decreasing load half-cycles of different loading magnitude (ΔK, R), as shown in the lower part of figure 4. The half-cycle theory (or half-wave theory) (refs. 7 to 10) states that the damage (or crack growth) caused by each half-cycle of either increasing or decreasing load is assumed to equal one-half the damage caused by a complete cycle of the same loading magnitude

(ΔK, R). This means that the damage caused by the complete cycle could be equally divided between the two phases of increasing and decreasing loads. The loading sequence thus can be resolved into half-cycle groups of increasing and decreasing loads (see lower part of fig. 3). Each half-cycle (either increasing or decreasing load) can then be considered as a half-cycle of the constant-amplitude cyclings under the same loading magnitude (ΔK, R) and can be computed separately in time sequence to estimate the corresponding damage. The half-cycle theory thus permits accurate evaluation of the load spectrum from a recorded load time history. If a_ℓ (ℓ = 1, 2, 3, . . .) is the final crack length after N_ℓ (ℓ = 1, 2, 3, . . .) random stress cyclings in the ℓth flight, then according to the half-cycle theory, a_ℓ may be calculated from

$$a_\ell = a_{\ell-1} + \sum_{i=1}^{2N_\ell} \frac{\delta a_i}{2} = a_{\ell-1} + \Delta a_\ell \tag{10}$$

with

$$\Delta a_\ell = \sum_{i=1}^{2N_\ell} \frac{\delta a_i}{2} = a_\ell - a_{\ell-1} \quad \text{and} \quad a_{1-1} = a_c^P \tag{11}$$

where $\delta a_i/2$ is the crack growth increment induced by the ith half-cycle under the loading magnitude ΔK_i and R_i; $\delta a_i/2$ is assumed to equal the crack growth increment induced by a half-cycle of the constant-amplitude stress cycle fatigue test under the same loading magnitude (ΔK_i, R_i). Thus, by using equations (6) to (9), $\delta a_i/2$ may be calculated from

$$\frac{\delta a_i}{2} = \frac{1}{2}\left[\frac{da}{dN}\right]_i = \frac{C}{2}\left[(K_{max})_i\right]^m (1 - R_i)^n = \frac{C}{2}(\Delta K_i)^m (1 - R_i)^{n-m} \tag{12}$$

The crack length, a, associated with ΔK_i (see eq. (8)) will be the summation of the initial crack length and all the crack growth increments created by all the previous half-cycles:

$$a = a_c^P + \sum_{j=1}^{i-1} \frac{\delta a_j}{2} \quad (i > 2) \tag{13}$$

Similar to the case of constant-amplitude stress cycling (see eq. (5)), the number of remaining flights F_ℓ (ℓ = 1, 2, 3, . . .) after the ℓth flight of random stress cycling may be calculated from

$$F_\ell = \frac{a_c^o - a_{\ell-1}}{\Delta a_\ell} = \frac{a_c^o - a_{\ell-1}}{a_\ell - a_{\ell-1}} = \frac{a_c^o - a_{\ell-1}}{\displaystyle\sum_{i=1}^{2N_\ell} \frac{\delta a_i}{2}} \tag{14}$$

Figure 4 graphically illustrates how to evaluate the crack growth increment $\delta a_i/2$ associated with the ith half-cycle of the random stress cycling by using the plots of ΔK_i as functions of da/dN for different values of R.

As mentioned previously, equations (5) and (14) both may give relatively accurate values for F_ℓ when the number of remaining flights is relatively low. When predicting large F_ℓ, equations (5) and (14) must be modified because Δa_ℓ increases with the flights accumulated.

New Equation for Remaining Flights

For the case of constant-amplitude stress cycling, the amount of crack growth Δa_ℓ ($\ell = 1, 2, 3, \ldots$) during the ℓth flight (N_ℓ cyclings) may be obtained by integrating equation (6):

$$\Delta a_\ell = C \left(AM_K \sigma_{max} \sqrt{\frac{\pi}{Q}} \right)^m (1 - R)^n N_\ell \left(a_{\ell-1} \right)^{m/2} \qquad (\ell = 1, 2, 3, \ldots) \qquad (15)$$

where equation (7) was used.

For simplicity, if σ_{max}, R, and N_ℓ remain the same for all the flights, then the following crack growth rates can be established by using equation (15), assuming $\Delta a_\ell / a_{\ell-1} \ll 1$:

$$\frac{\Delta a_2}{\Delta a_1} = \left(\frac{a_1}{a_c^P} \right)^{m/2} = \left(\frac{a_c^P + \Delta a_1}{a_c^P} \right)^{m/2} = 1 + \frac{m}{2} \frac{\Delta a_1}{a_c^P} + \ldots \qquad (16)$$

$$\frac{\Delta a_3}{\Delta a_1} = \left(\frac{a_2}{a_c^P} \right)^{m/2} = \left(\frac{a_c^P + \Delta a_1 + \Delta a_2}{a_c^P} \right)^{m/2} = 1 + 2 \left(\frac{m}{2} \frac{\Delta a_1}{a_c^P} \right) + \ldots \qquad (17)$$

$$\frac{\Delta a_4}{\Delta a_1} = \left(\frac{a_3}{a_c^P} \right)^{m/2} = \left(\frac{a_c^P + \Delta a_1 + \Delta a_2 + \Delta a_3}{a_c^P} \right)^{m/2} = 1 + 3 \left(\frac{m}{2} \frac{\Delta a_1}{a_c^P} \right) + \ldots \qquad (18)$$

$$\vdots$$

$$\frac{\Delta a_\ell}{\Delta a_1} = \left(\frac{a_{\ell-1}}{a_c^P} \right)^{m/2} = \left(\frac{a_c^P + \Delta a_1 + \Delta a_2 + \Delta a_3 + \ldots + \Delta a_{\ell-1}}{a_c^P} \right)^{m/2}$$

$$= 1 + (\ell-1) \left(\frac{m}{2} \frac{\Delta a_1}{a_c^P} \right) + \ldots \qquad (19)$$

8

If the available crack size, $a_c^O - a_c^P$, can allow $\bar{F}_1$ number of remaining flights, then

$$\frac{a_c^O - a_c^P}{\Delta a_1} = \frac{\overbrace{\Delta a_1 + \Delta a_2 + \Delta a_3 + \ldots + \Delta a_\ell + \ldots + \Delta a_{\bar{F}_1}}^{\bar{F}_1 \text{ terms}}}{\Delta a_1} \quad (20)$$

where the left-hand side is F_1, the number of remaining flights predicted by assuming that $\Delta a_1 = \Delta a_2 = \Delta a_3 = \ldots = \Delta a_\ell = \ldots = \Delta a_{F_1}$ (see eq. (14) for $\ell = 1$). Substituting equations (14) and (16) to (19) into equation (20),

$$F_1 = \overbrace{(1 + 1 + 1 + \ldots + 1)}^{\bar{F}_1 \text{ terms}} + \frac{m}{2}\frac{\Delta a_1}{a_c^P}\overbrace{[1 + 2 + 3 + \ldots + (\bar{F}_1 - 1)]}^{(\bar{F}_1 - 1) \text{ terms}} \quad (21)$$

or

$$F_1 = \bar{F}_1 + \frac{m}{2}\frac{\Delta a_1}{a_c^P}\frac{(\bar{F}_1 - 1)[(\bar{F}_1 - 1) + 1]}{2} \quad (22)$$

Equation (22) may be rearranged into the form

$$\frac{m}{4}\frac{\Delta a_1}{a_c^P}\bar{F}_1^2 + \left(1 - \frac{m}{4}\frac{\Delta a_1}{a_c^P}\right)\bar{F}_1 - F_1 = 0 \quad (23)$$

Solving for $\bar{F}_1$,

$$\bar{F}_1 = \frac{2a_c^P}{m\,\Delta a_1}\left(\sqrt{1 + \frac{m\,\Delta a_1}{a_c^P}F_1} - 1\right) \quad (24)$$

which gives the relationship between $\bar{F}_1$ and F_1.

If the prediction of the number of remaining flights is based on the crack growth Δa_ℓ that occurred during the ℓth flight, equation (24) takes the form

$$\bar{F}_\ell = \frac{2a_{\ell-1}}{m\,\Delta a_\ell}\left(\sqrt{1 + \frac{m\,\Delta a_\ell}{a_{\ell-1}}F_\ell} - 1\right) \quad (25)$$

Equations (24) and (25) both apply to the case of constant-amplitude stress cycling. However, they may be used for the case of variable-amplitude stress cycling without introducing significant error. Figure 5 shows the plot of equation (24) (that is, $\bar{F}_1$ as a function of F_1) for $m = 3.6$ (Inconel 718 alloy) and $\Delta a_1/a_c^P = 0.01814$ for

the example described in the following sections. Some typical values of $\bar{F}_1$ and F_1 are compared in the following tabulation:

F_1:	1	10	50	100	150	200	500	1000
$\bar{F}_1$:	1	9	33	53	70	84	147	218

The ratio $\bar{F}_1/F_1$ is 0.53 for $F_1 = 100$ and decreases to 0.218 for $F_1 = 1000$. Thus, equation (5) certainly overpredicts the number of remaining flights, and safety factors ranging from 2 to 4 must be used depending on the range of the value of F_1.

EXAMPLE PROBLEM

For this report, the example problem chosen for the fatigue analysis using the half-cycle method is the severe fatigue problem of the three hooks of the NASA B-52-008 carrier aircraft pylon used to carry the space shuttle solid rocket booster drop test vehicle (SRB/DTV) shown in figure 6. The 49,000-lb SRB/DTV was attached to the pylon with one front hook and two rear hooks (see fig. 6). The SRB/DTV was carried up to high altitude and released to test the performance of the solid rocket booster main parachute. The shapes of the front hook and the two rear hooks are shown in figures 7 and 8, respectively. The front hook is made of Inconel 718 alloy and the two rear hooks of AMAX MP35N alloy (AMAX Specialty Corporation). Table 1 shows material properties of the two alloys. Because of the great weight of the SRB/DTV, the three hooks had serious fatigue life problems. Fracture mechanics and the half-cycle method can be applied to predict the service life (number of remaining flights) of the three hooks that carried the SRB/DTV. Reference 10 presents the detailed fatigue analysis of the NASA B-52 aircraft pylon major components.

Critical Stress Points

Before conducting fatigue-crack growth analysis, the locations of the critical stress points for the three hooks had to be determined. This was done by performing NASTRAN finite-element stress analysis of the three hooks (ref. 11). The critical stress point of each hook is located at the inner circular boundary of the hook. Figures 7 and 8 show the exact locations of the critical stress points of the three hooks. Through the NASTRAN stress analysis, the relationships between the stress at the critical stress point and the hook loads were established as

$$\sigma_1 = 7.3522 \times 10^{-3} \, V_A \qquad \text{for front hook} \qquad (26)$$

$$\sigma_2 = 5.8442 \times 10^{-3} \, V_{BL} \qquad \text{for left rear hook} \qquad (27)$$

$$\sigma_3 = 5.8442 \times 10^{-3} \, V_{BR} \qquad \text{for right rear hook} \qquad (28)$$

where σ_1, σ_2, and σ_3 are respectively the stresses (in kips, or 10^3 lb, per square inch (ksi)) at the critical stress points of the front hook, left rear hook, and

right rear hook, and V_A, V_{BL}, and V_{BR} are the corresponding hook vertical loads in pounds. During proof load tests and during flight, V_A, V_{BL}, and V_{BR} were measured by means of strain gages installed near the critical stress points of the hooks (refs. 10 and 11). Equations (26) to (28) were used to generate stress cycles for the fatigue-crack growth analysis using the strain-gage-measured values of V_A, V_{BL}, and V_{BR}.

Initial and Operational Crack Sizes

During the proof load tests, the three hooks were loaded to their respective peak proof loads to establish the initial crack size a_c^P for each critical stress point. The peak proof stresses σ_i^* (i = 1, 2, 3) at the critical stress points induced by the peak proof hook loads may be calculated from equations (26) to (28). The proof crack size a_c^P at the critical point of each hook established by the proof load tests may be calculated from equation (1) by setting $K_I = K_{I_C}$:

$$a_c^P = \frac{Q}{\pi}\left(\frac{K_{I_C}}{AM_K\sigma^*}\right)^2 \tag{29}$$

where A = 1.12 for the surface crack, $M_K = 1$ (which was obtained from the lower right plot of figure 1 for a/t << 1 because the depth of the crack is very small compared with the depth of the hook), and the value of Q, the surface flow shape and plasticity factor, will be determined as follows.

The surface crack is assumed to be semielliptical in shape with an aspect ratio of a/2c = 1/4. (This value is based on the observation of surface cracks of the fractured old rear hooks.) Taking a/2c = 1/4 and $\sigma_\infty/\sigma_Y = \sigma_i^*/\sigma_Y = 1$ (because the growth of plastic zones around the critical stress points was neglected, the values of $\sigma_i^{\bullet}$ calculated for the three hooks slightly exceeded the corresponding yield stresses σ_Y), the curve for $\sigma_\infty/\sigma_Y = 1$ in the lower left plots of figure 1 gives Q = 1.25.

If the peak value of the stress cycles during operation (or flight) is $f\sigma_i^*$, where f is the operational peak stress factor (f < 1), then the operational limit crack size a_c^O may be calculated from

$$a_c^O = \frac{Q}{\pi}\left(\frac{K_{I_C}}{AM_Kf\sigma_i^*}\right)^2 = \frac{a_c^P}{f^2} \tag{30}$$

Part of table 2 shows the peak proof hook loads, the peak proof stresses σ_i^*, and the proof crack sizes a_c^P at the critical stess points. Note that for all three hooks, σ_i^* exceeded the failure stresses σ_U of the hook materials (see table 1), yet the three hooks did not fail during the proof load tests. The reason is that equations (25) to (27), established by the NASTRAN analysis, are for a purely elastic

case without consideration of plastic deformations. In reality the plastic zone can develop around the critical stress point, and therefore the hook can actually carry a greater load than the brittle failure load. In the present fatigue-crack growth analysis, only the elastic case is considered.

Load Spectra

To perform the fatigue-crack growth analysis, the load spectra (stress cycles) for the three critical points of the hooks must be obtained first. Using the strain-gage-measured values of the three hook loads, V_A, V_{BL}, and V_{BR}, during the first test flight, the three stresses σ_i ($i = 1$, 2, 3) may be calculated by using equations (26) to (28). Figures 9 to 11 (ref. 10) show portions of the loading histories (load spectra) calculated for the critical stress points of the three hooks during a takeoff run. Those load spectra were obtained by filtering the original load spectra down to 5 Hz to eliminate the small-amplitude high-frequency stess cycles that are considered unimportant in the present fatigue life analysis. Notice that the load spectra for all three critical stress points exhibit a high degree of random cycling.

Calculations of Crack Growth

To apply the half-cycle method, the load spectra (see figs. 9 to 11) were first resolved into a series of half-cycles of increasing and decreasing loads of different loading magnitude (ΔK, R) (see fig. 3). The crack growth increments $\delta a_i/2$ per half-cycle were calculated from equation (12) in time sequence and summed (using eq. (10)) to give the total amount of crack growth per flight for each critical stress point. Finally, equations (14) and (25) were used to calculate the number of remaining flights associated with each critical stress point. It must be emphasized that in using the half-cycle method, every half-cycle of different stress amplitude in the load spectrum is calculated, and thus the half-cycle method can give an accurate evaluation of the fatigue-crack growth as compared with, say, the exceedence-count method (for which some of the stress peaks lying below the mean line could be missed).

Results

Figures 12 to 14, taken from reference 10, show the fatigue-crack growth curves calculated for the three critical stress points for the first test flight; the maneuver transition points are indicated. Note that for the three hooks, the fatigue-crack growth rate is greatest during the initial stage of taxiing and the takeoff run and becomes very low during cruising because of relatively low-amplitude stress cyclings. Table 2 lists the amount of crack growth Δa_1, operational peak stress factor f, operational crack size a_c^o, and remaining flights F_1 and $\bar{F}_1$ calculated respectively from equations (14) and (24). Figure 15 shows the plots of F_1 and $\bar{F}_1$ as functions of f for the three hooks. Note that the over-prediction of remaining flights based on F_1 (eq. (14)) becomes more pronounced as the number of remaining flights increases. The arrows in figure 15 indicate the

actual operational peak load levels. At these load levels, safety factors must be in the range of 2 to 2.5 if F_1 is used instead of $\bar{F}_1$.

CONCLUSION

Fracture mechanics and the half-cycle method were applied to the service life analysis of aircraft structural components. The initial crack sizes at the critical stress points of the structural components were determined by using proof load tests. The random stress cycle fatigue-crack growth rates were calculated using the half-cycle method. A new equation was developed for calculating the number of remaining flights for the structural components. The newly developed equation predicted the number of remaining flights more accurately (a much lower number) than did the conventional equation (which is based on the assumption that the amount of crack growth per flight remains constant).

REFERENCES

1. Donaldson, D.R.; and Anderson, W.F.: Crack Propagation Behavior of Some Airframe Materials. Proceedings of the Crack Propagation Symposium, vol. 2, Cranfield, Sept. 1961.

2. Butler, J.P.: The Material Selection and Structural Development Process for Aircraft Structural Integrity Under Fatigue Conditions. AFFDL-TR-70-144, Conference Proceedings, Air Force Conference, Miami, Florida, December 15-18, 1969.

3. Astley, W.; and Scott, J.: Engineering Practice to Avoid Stress Corrosion Cracking. (The Environment Encountered in Aircraft Service.) AGARD Conference Proceedings No. 53.

4. Forman, R.G.; Kearney, V.E.; and Engle, R.M.: Numerical Analysis of Crack Propagation in Cycle Loaded Structures. J. Basic Engineering, Trans. A.S.M.E. D 89, 1967, p. 459.

5. Walker, E.K.: The Effect of Stress Ratio During Crack Propagation and Fatigue for 2024-T3 and 7075-T6 Aluminum, Effects of Environments and Complex Load History on Fatigue Life. ASTM-STP 462, 1970, p. 1.

6. Schijve, J.: Four Lectures on Fatigue Crack Growth. Engineering Fracture Mechanics, vol. II, Pergamon Press, New York, 1979, pp. 167-221.

7. Starkey, W.L.; and Marco, S.M.: Effects of Complex Stress-Time Cycles on the Fatigue Properties of Metals. Trans. A.S.M.E., Aug. 1957, pp. 1329-1336.

8. Incarbone, C.: Fatigue Research on Specific Design Problems. Fatigue of Aircraft Structures, Proceedings of the Symposium held in Paris, 16th-18th May 1961, W. Barrois and E.L. Ripley, eds., Pergamon Press, New York, 1963, pp. 209-217.

9. Smith, S.H.: Fatigue Crack Growth Under Axial Narrow and Broad Band Random Loading. Acoustic Fatigue in Aerospace Structures, Syracuse University Press, 1965, p. 331.

10. Ko, William L.; Carter, Alan L.; Totton, William W.; and Ficke, Jules M.: Application of Fracture Mechanics and the Half-Cycle Method to the Prediction of Fatigue Life of B-52 Aircraft Pylon Components. NASA TM-88277, 1987.

11. Ko, William L.; and Schuster, Lawrence S.: Stress Analyses of B-52 Pylon Hooks. NASA TM-84924, 1985.

TABLE 1. — MATERIAL PROPERTIES OF FRONT AND REAR HOOKS

Stress point	Part name	Material	σ_U (ksi)	σ_Y (ksi)	$\tau_U{}^a$ (ksi)	$C \left(\dfrac{\text{in}}{\text{cycle}} (\text{ksi } \sqrt{\text{in}})^{-m}\right)$	m	n	K_{I_C} (ksi $\sqrt{\text{in}}$)
σ_1	Front hook	Inconel 718 alloy	175	145	135	9.220×10^{-12}	3.6	2.16	125
σ_2	New left rear hook	AMAX MP35N alloy	250	235	141	2.944×10^{-11}	3.24	1.69	124
σ_3	New right rear hook	AMAX MP35N alloy	250	235	141	2.944×10^{-11}	3.24	1.69	124

^{a} τ_U is the ultimate sheer strength.

TABLE 2. — CRACK SIZES AND REMAINING FLIGHTS

Hook	Proof hook load (lb)	Proof stress at critical stress point, σ_i (ksi)	Proof crack size a_c^p (in)	Crack growth Δa_1 (in)	Operational peak stress factor f	Operational crack size $a_c^o = \dfrac{a_c^p}{f^2}$ (in)	Remaining flights F_1	Remaining flights $\bar{F}_1$
Front hook	$V_A = 36{,}520$	268.502	0.0990	0.0018295	0.5450	0.3333	128	63
Left rear hook	$V_{BL} = 44{,}110$	257.786	0.0734	0.0005887	0.5946	0.2076	227	91
Right rear hook	$V_{BR} = 44{,}230$	258.487	0.0730	0.0007705	0.5986	0.2037	169	75

Figure 1. Three types of cracks and the plots of surface flaw shape factor and flaw magnification factor.
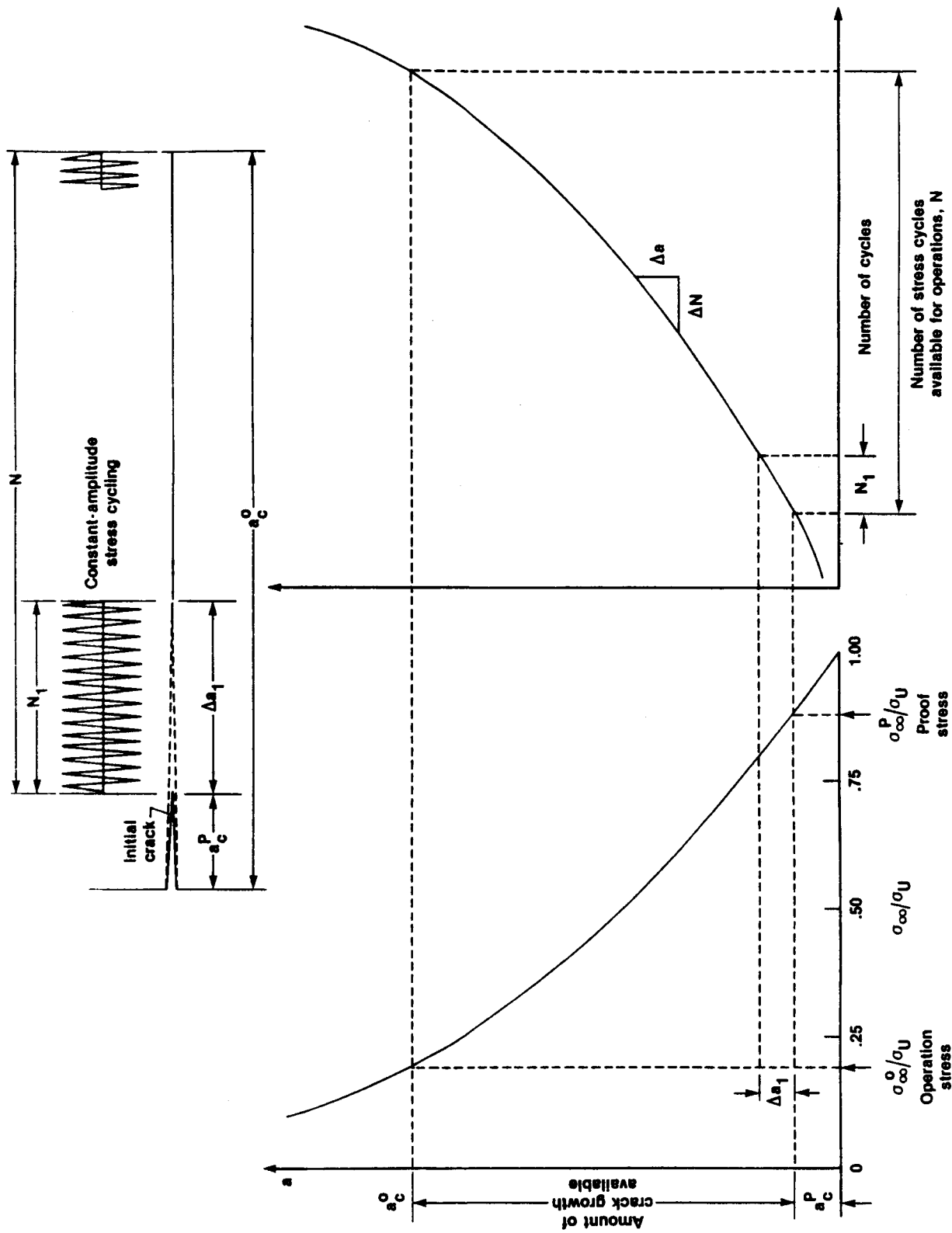
Figure 2. Crack length as functions of applied stress and number of cycles.
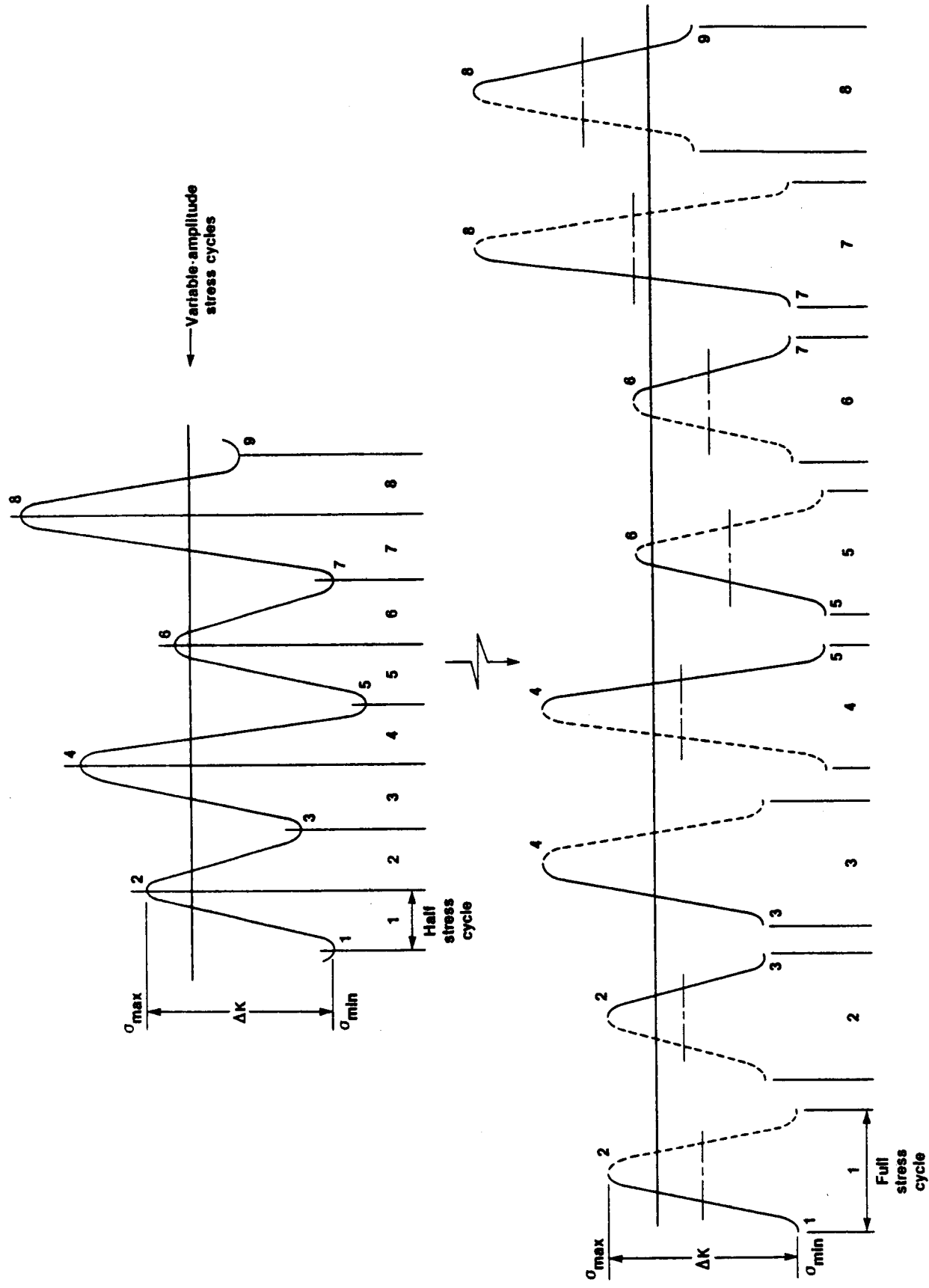
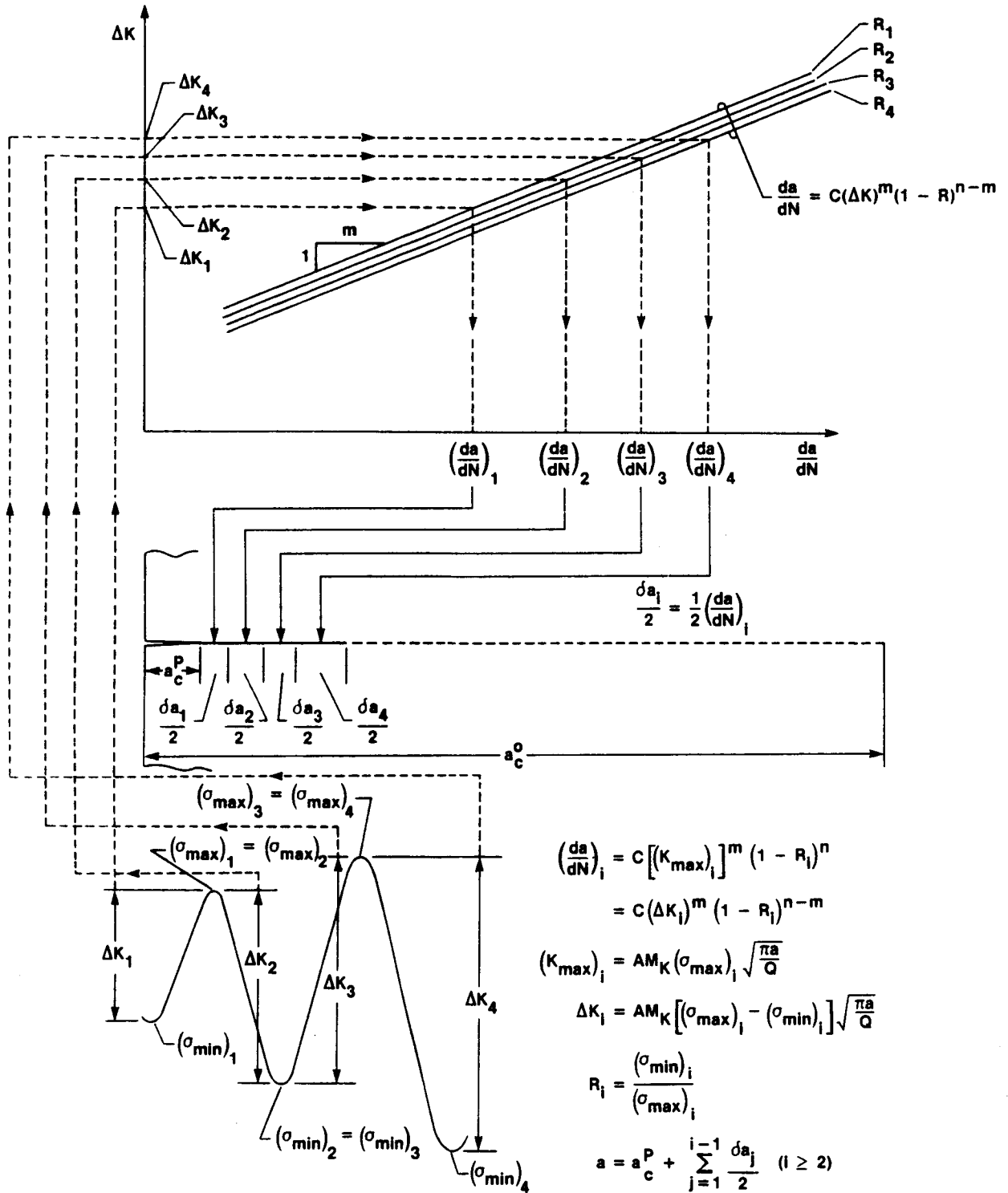Figure 3. Resolution of random stress cycles into half stress cycles of different stress ranges.

Figure 4. Graphical evaluation of crack increments for random stress cycles using the half-cycle method.
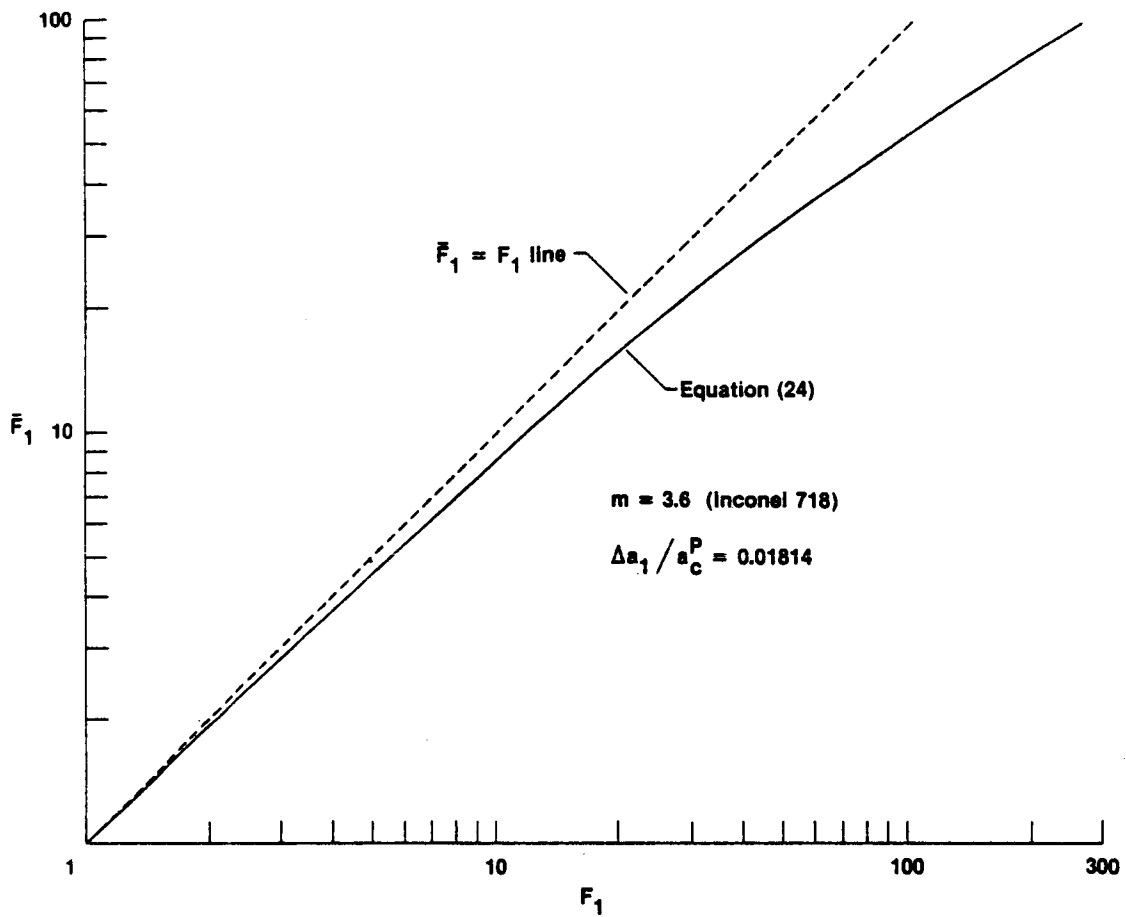
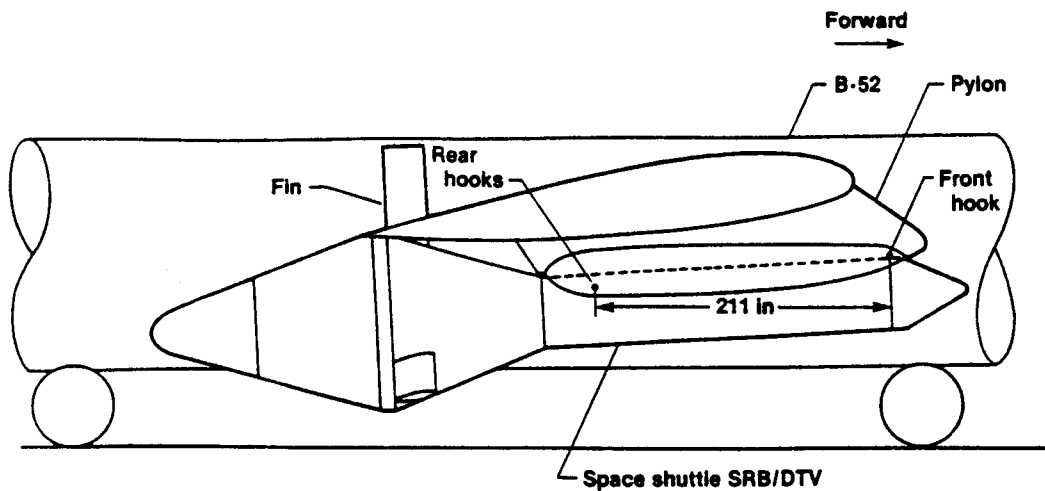*Figure 5. Number of remaining flights predicted from Ko equation of remaining flights.*

Figure 6. Geometry of space shuttle solid rocket booster drop test vehicle (SRB/DTV) attached to B-52 pylon (view looking inboard from right side).

20
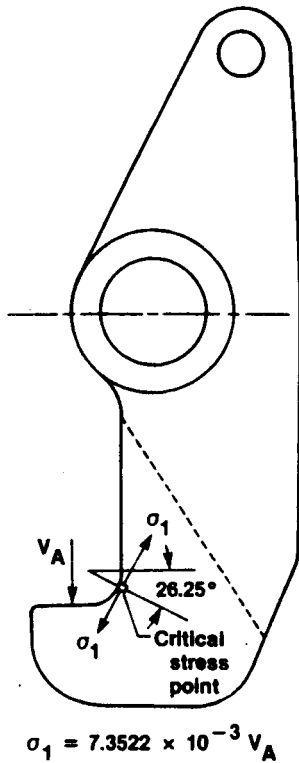
Figure 7. Front hook and the location of critical stress point σ_1.

$$\sigma_1 = 7.3522 \times 10^{-3} V_A$$

$$\sigma_2 = 5.8442 \times 10^{-3} V_{BL}$$
$$\sigma_3 = 5.8442 \times 10^{-3} V_{BR}$$
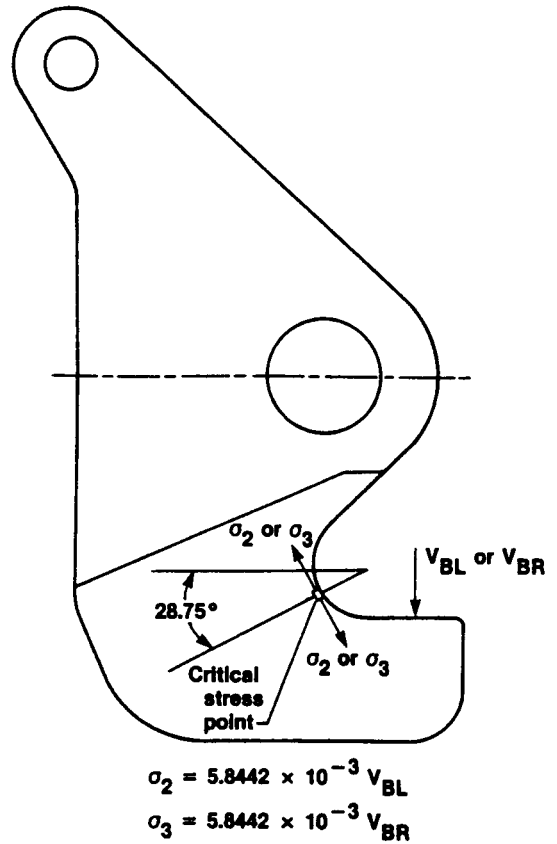
Figure 8. Rear hook (left or right) and the location of critical stress point (σ_2 or σ_3).

$$\sigma_1 = 7.3522 \times 10^{-3} V_A$$
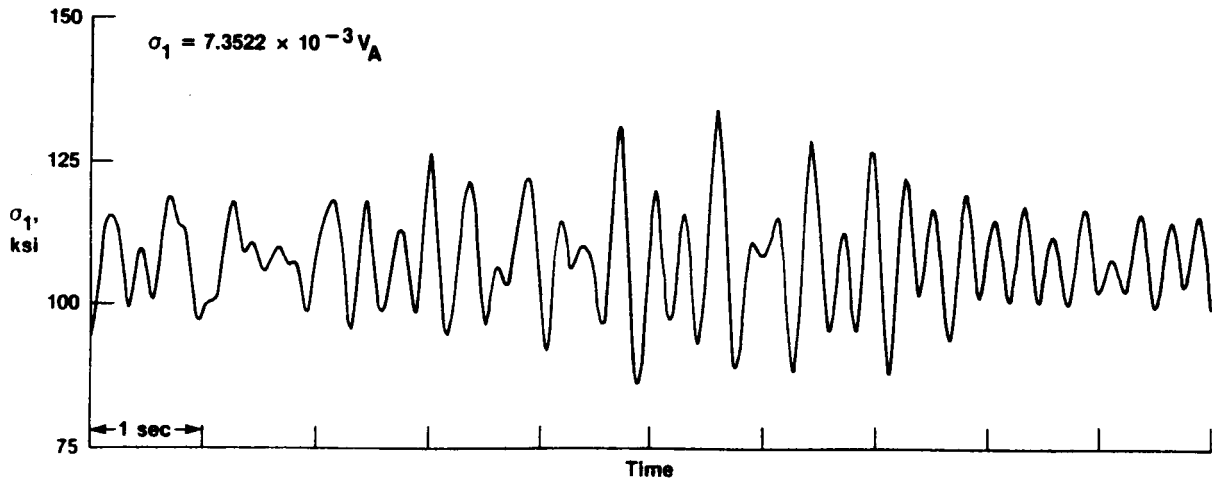
Figure 9. Stress cycles for critical stress point σ_1 at front hook.
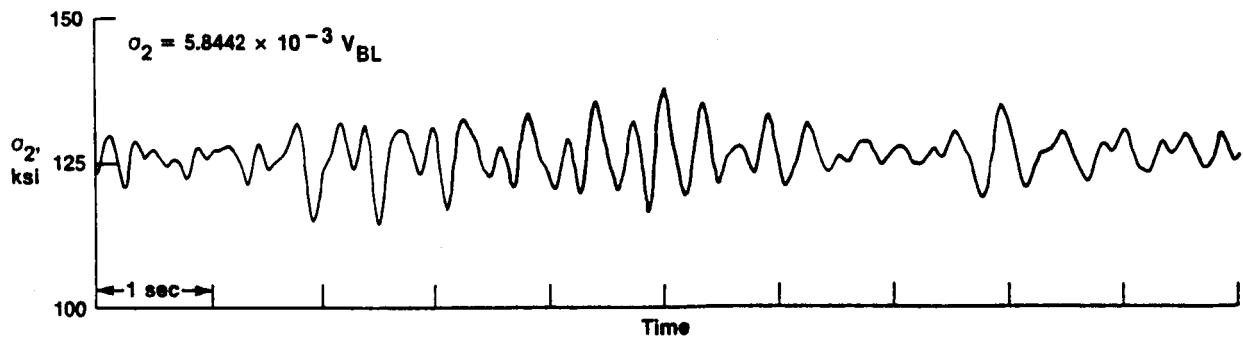
Figure 10. *Stress cycles for critical stress point* σ_2 *at left rear hook.*

$\sigma_2 = 5.8442 \times 10^{-3} V_{BL}$
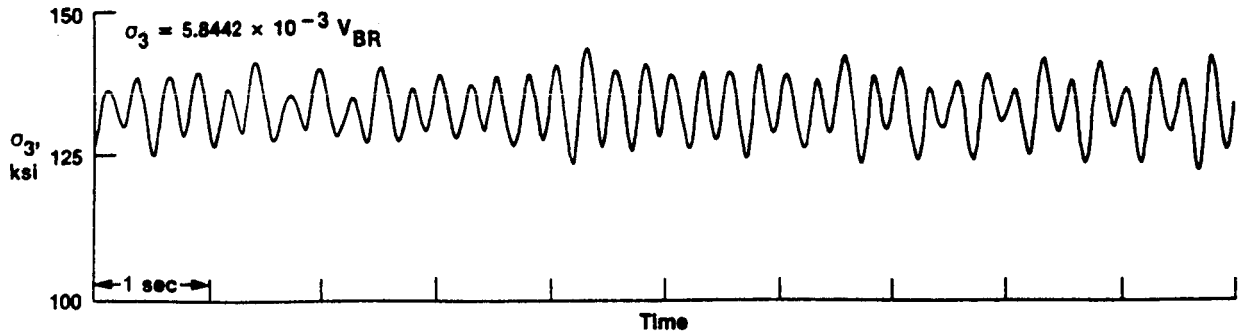
Figure 11. *Stress cycles for critical stress point* σ_3 *at right rear hook.*

$\sigma_3 = 5.8442 \times 10^{-3} V_{BR}$
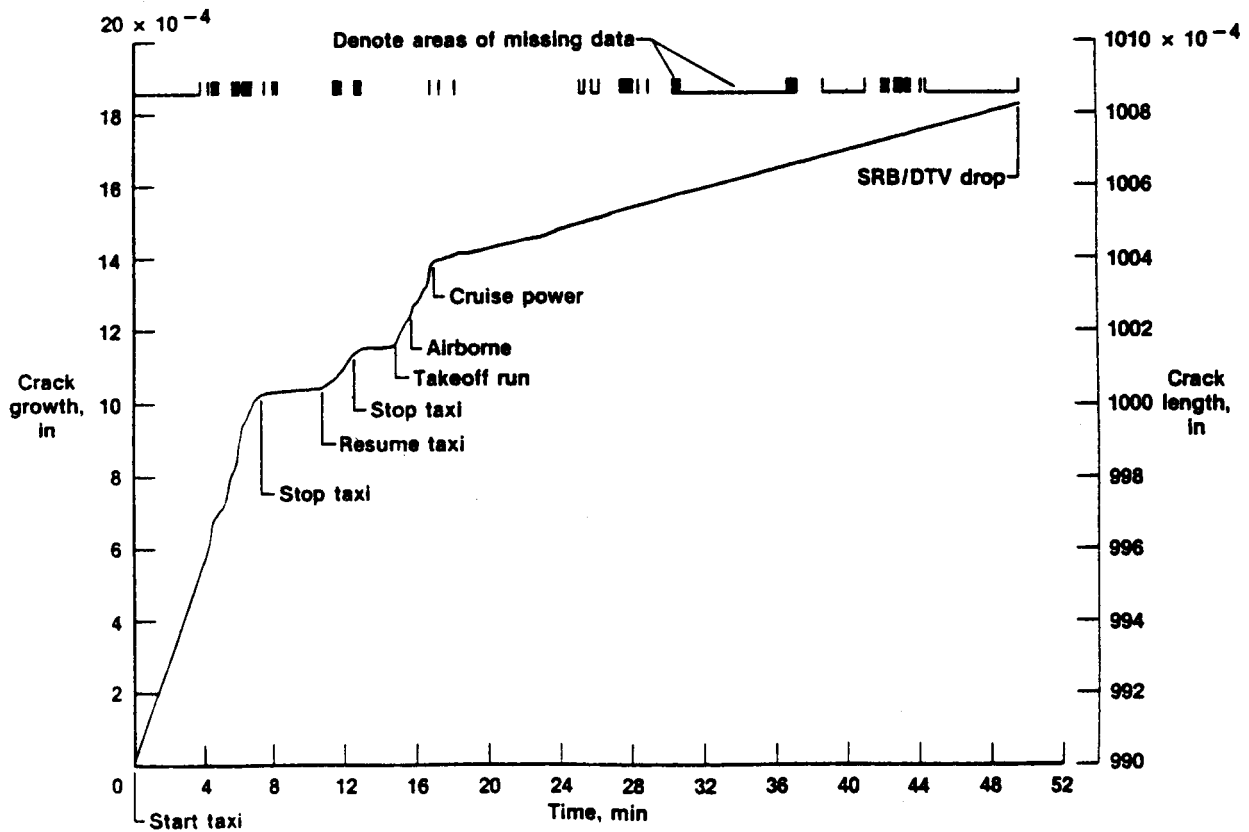
Figure 12. *Crack growth curve for stress point 1* (σ_1), *flight 1.*
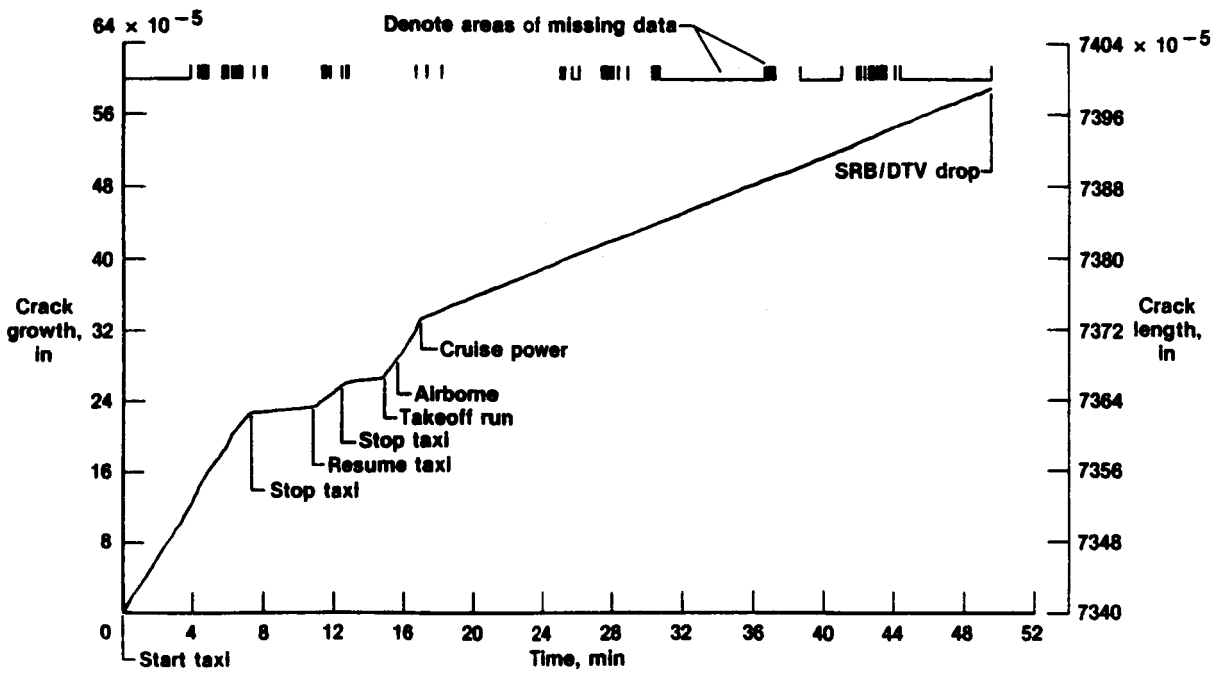
Figure 13. **Crack growth curve for stress point 2 (σ_2), flight 1.**
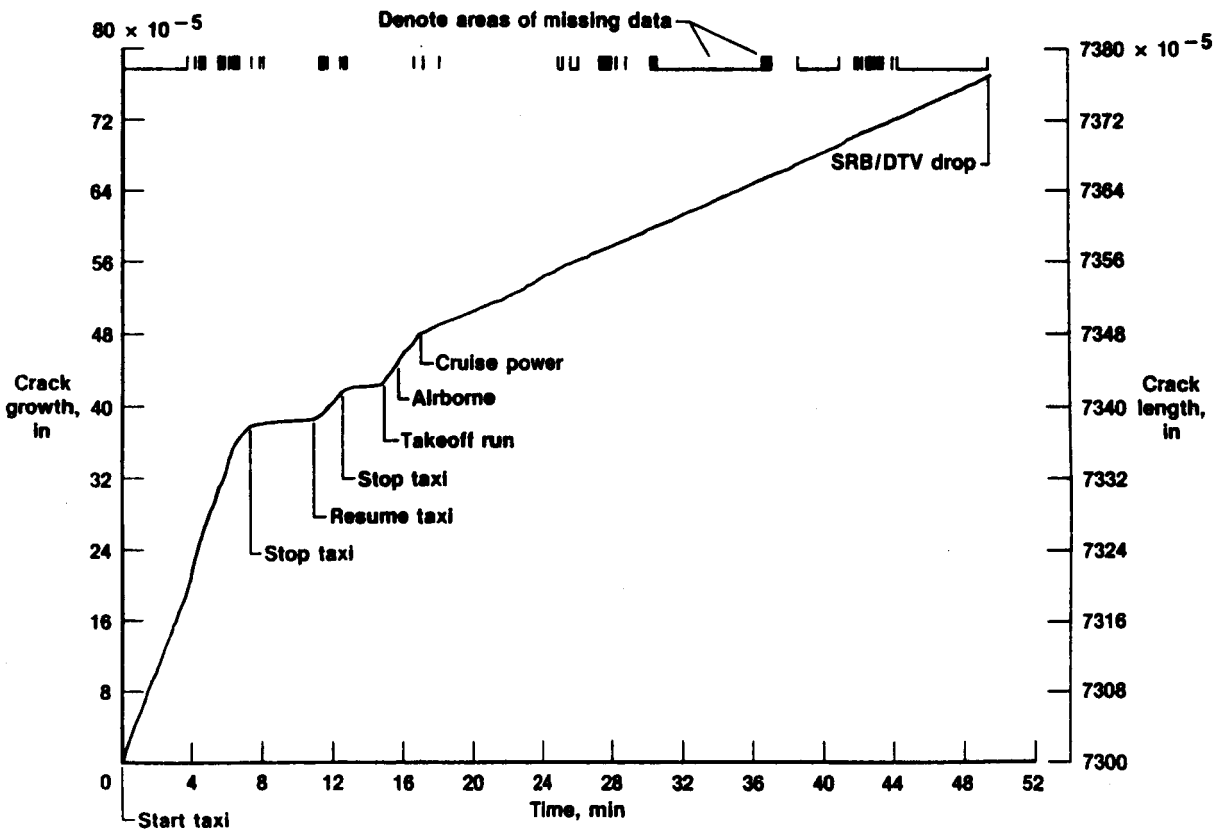

Figure 14. **Crack growth curve for stress point 3 (σ_3), flight 1.**
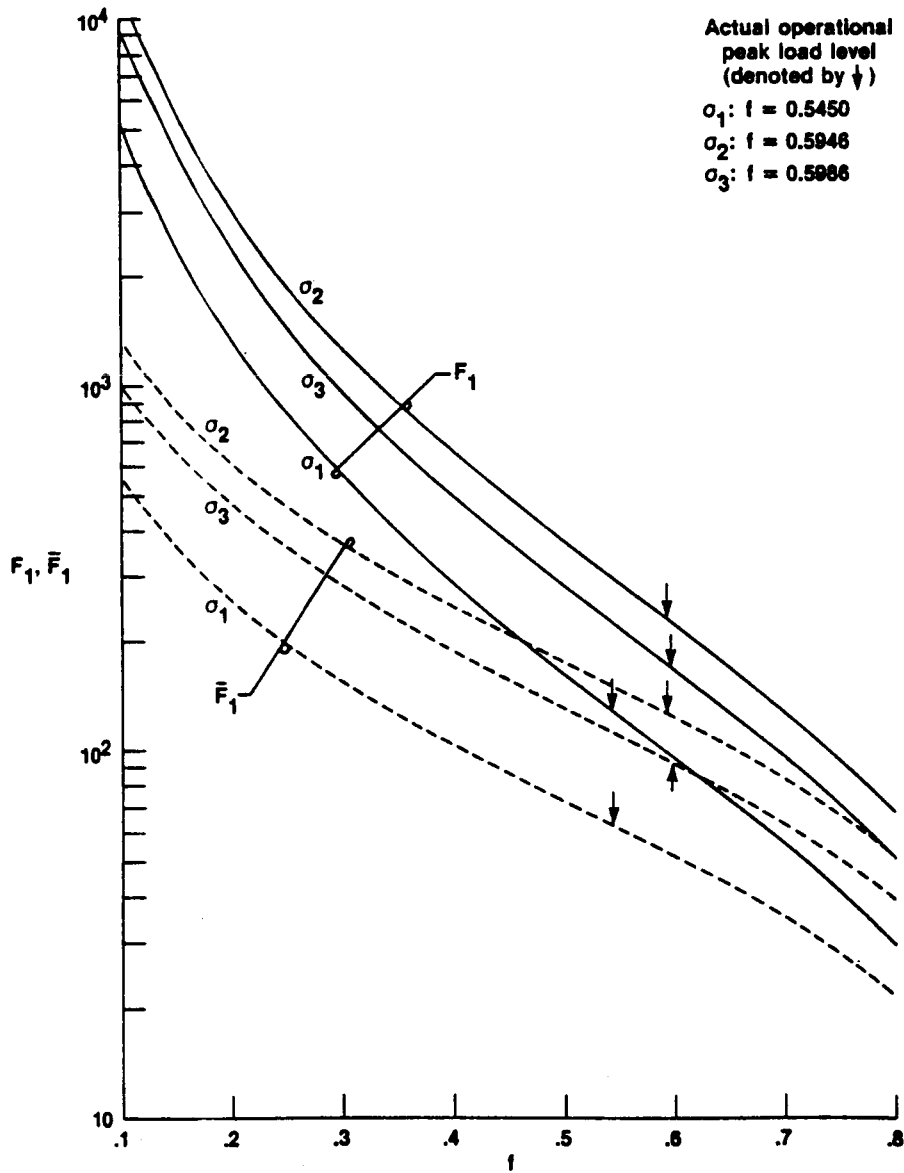
Figure 15. *Number of remaining flights as functions of operational peak stress factor.*

1. Report No. NASA TM-86812	2. Government Accession No.	3. Recipient's Catalog No.

4. Title and Subtitle
  Prediction of Service Life of Aircraft Structural
  Components Using the Half-Cycle Method
		5. Report Date
		  May 1987

		6. Performing Organization Code

7. Author(s)
  William L. Ko
		8. Performing Organization Report No.
		  H-1352

		10. Work Unit No. RTOP 505-43-31

9. Performing Organization Name and Address
  NASA Ames Research Center
  Dryden Flight Research Facility
  P.O. Box 273
  Edwards, CA 93523-5000
		11. Contract or Grant No.

		13. Type of Report and Period Covered Technical Memorandum

12. Sponsoring Agency Name and Address
  National Aeronautics and Space Administration
  Washington, DC 20546		

		14. Sponsoring Agency Code

15. Supplementary Notes

16. Abstract

    The service life of aircraft structural components under-
going random stress cycling was analyzed by the application of
fracture mechanics. The initial crack sizes at the critical
stress points for the fatique-crack growth analysis were estab-
lished through proof load tests. The fatique-crack growth rates
for random stress cycles were calculated using the half-cycle
method. A new equation was developed for calculating the number
of remaining flights for the structural components. The number
of remaining flights predicted by the new equation is much lower
than that predicted by the conventional equation.

17. Key Words (Suggested by Author(s))
 	
  Fatigue life
  Fracture Mechanics
  Half-cycle method
  Random cycling
  Service life prediction
	18. Distribution Statement
	
	  Unclassified — Unlimited
	
	  Subject category 39		

19. Security Classif. (of this report)
  Unclassified
	20. Security Classif. (of this page)
	  Unclassified
		21. No. of Pages
		  25
			22. Price*
			  A02